# Predicting Frictional Properties of Graphene Kirigami Using Molecular Dynamics and Neural Networks

*Designs for a negative friction coefficient.*

Mikkel Metzsch Jensen


Thesis submitted for the degree of
Master in Computational Science: Materials Science
60 credits

Department of Physics
Faculty of mathematics and natural sciences

UNIVERSITY OF OSLO

Spring 2023

# Predicting Frictional Properties of Graphene Kirigami Using Molecular Dynamics and Neural Networks

*Designs for a negative friction coefficient.*

Mikkel Metzsch Jensen

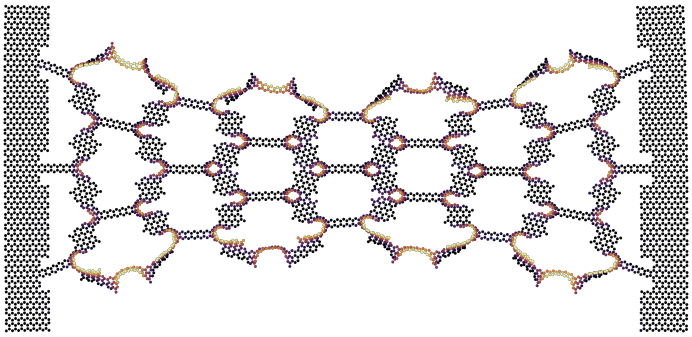

Predicting Frictional Properties of Graphene Kirigami Using Molecular Dynamics and Neural Networks

http://www.duo.uio.no/

Printed: Reprosentralen, University of Oslo

# Abstract

Abstract.

# Acknowledgments

Acknowledgments.

# List of Symbols

$F_N$ Normal force (normal load)

# Acronyms

**CNN** Convolutional Neural Network. 11, 13

**EMA** Exponetial Moving Average. 10

**MD** Molecular Dynamics. 1, 2, 3, 7

**ML** Machine Learning. 2, 3

**MSE** Mean Squared Error. 8

**RMSProp** Root Mean Square Propagation. 10

**SGD** Stochastic gradient descent. 9

# Contents

# Chapter 1

# Introduction

## 1.1 Motivation

Friction is the force that prevents the relative motion of objects in contact. Even though the everyday person might not be familiar with the term *friction* we recognize it as the inherent resistance to sliding motion. Some surfaces appear slippery and some rough, and we know intuitively that sliding down a snow-covered hill is much more exciting than its grassy counterpart. Without friction, it would not be possible to walk across a flat surface, lean against the wall without falling over or secure an object by the use of nails or screws [p. 5] [1]. It is probably safe to say that the concept of friction is integrated into our everyday life to such an extent that most people take it for granted. However, the efforts to control friction date back to the early civilization (3500 B.C.) with the use of the wheel and lubricants to reduce friction in translational motion [2]. Today, friction is considered a part of the wider field *tribology* derived from the Greek word *Tribos* meaning "rubbing" and includes the science of friction, wear and lubrication [2]. The most compelling motivation to study tribology is ultimately to gain full control of friction and wear for various technical applications. Especially, reducing friction is of great interest as this has tremendous advantages for energy efficiency. It has been reported that tribological problems have a significant potential for economic and environmental improvements [3]:

> "On global scale, these savings would amount to 1.4% of the GDP annually and 8.7% of the total energy consumption in the long term." [4].

On the other hand, the reduction of friction is not the only sensible application for tribological studies. Controlling frictional properties, besides minimization, might be of interest in the development of a grasping robot where finetuned object handling is required. While achieving a certain "constant" friction response is readily obtained through appropriate material choices during manufacturing, we are yet to unlock the capabilities to alter friction dynamically on the go. One example from nature inspiring us to think along these lines are the gecko feet. More precisely, the Tokay gecko has received a lot of attention in scientific studies aiming to unravel the underlying mechanism of its "togglable" adhesion properties. Although geckos can produce large adhesive forces, they retain the ability to remove their feet from an attachment surface at will [5]. This makes the gecko able to achieve a high adhesion on the feet when climbing a vertical surface while lifting it for the next step remains relatively effortless. For a grasping robot, we might consider an analog frictional concept of a surface material that can change from slippery to rough on demand depending on specific tasks.

In recent years an increasing amount of interest has gone into the studies of the microscopic origin of friction, due to the increased possibilities in surface preparation and the development of nanoscale experimental methods. Nano-friction is also of great concern for the field of nano-machining where the frictional properties between the tool and the workpiece dictate machining charascteristics [3]. With concurrent progress in computational power and development of Molecular Dynamics (MD), numerical investigations serve as an invaluable tool tool for getting insight into the nanoscale mechanics associated with friction. This simulation-based approach can be considered as a "numerical experiment" enabling us to create and probe a variety of high-complexity systems which are still out of reach for modern experimental methods.

In materials science such MD-based numerical studies have been used to explore the concept of so-called *metamaterials* where material compositions are designed meticulously to enhance certain physical properties [6–11]. This is often achieved either by intertwining different material types or removing certain regions completely.

In recent papers by Hanakata et al. [6, 7] numerical studies have showcased that the mechanical properties of a graphene sheet, yield stress and yield strain, can be altered through the introduction of so-called *kirigami* inspired cuts into the sheet. Kirigami is a variation of origami where the paper is cut additionally to being folded. While these methods originate as an art form, aiming to produce various artistic objects, they have proven to be applicable in a wide range of fields such as optics, physics, biology, chemistry and engineering [12]. Various forms of stimuli enable direct 2D to 3D transformations through folding, bending, and twisting of microstructures. While original human designs have contributed to specific scientific applications in the past, the future of this field is highly driven by the question of how to generate new designs optimized for certain physical properties. However, the complexity of such systems and the associated design space make for seemingly intractable problems ruling out analytic solutions.

Earlier architecture design approaches such as bioinspiration, looking at gecko feet for instance, and Edisonian, based on trial and error, generally rely on prior knowledge and an experienced designer [9]. While the Edisonian approach is certainly more feasible through numerical studies than real-world experiments, the number of combinations in the design space rather quickly becomes too large for a systematic search, even when considering the simulation time on modern-day hardware. However, this computational time constraint can be relaxed by the use of machine learning (ML) which has proven successful in the establishment of a mapping from the design space to physical properties of interest. This gives rise to two new styles of design approaches: One, by utilizing the prediction from a trained network we can skip the MD simulations altogether resulting in an *accelerated search* of designs. This can be further improved by guiding the search accordingly to the most promising candidates, for instance, as done with the *genetic algorithm* which suggests new designs based on mutation and crossing of the best candidates so far. Another more sophisticated approach is through generative methods such as *Generative Adversarial Networks* (GAN) or diffusion models used in state-of-the-art AI systems such as OpenAI's DALL·E2 or Midjourney SOURCE?. By working with a so-called *encoder-decoder* network structure, one can build a model that reverses the prediction process. That is, the model predicts a design from a set of physical target properties. In the papers by Hanakata et al. both the *accelerated search* and the *inverse design* approach was proven successful to create novel metamaterial kirigami designs with the graphene sheet.

Hanakata et al. attribute the variety in yield properties to the non-linear effects arising from the out-of-plane buckling of the sheet. Since it is generally accepted that the surface roughness is of great importance for frictional properties it can be hypothesized that the kirigami cut and stretch procedure can also be exploited for the design of frictional metamaterials. For certain designs, we might hope to find a relationship between the stretching of the sheet and frictional properties. If significant, this could give rise to a control of friction behavior beyond manufacturing. For instance, the grasping robot might apply such a material as artificial skin for which stretching or relaxing of the surface could result in a changeable friction strength; Slippery and smooth when interacting with people and rough and firmly gripping when moving heavy objects. In addition, a possible coupling between stretch and the normal load through a nanomachine design would allow for an altered friction coefficient. This invites the idea of non-linear friction coefficients which might in theory also take on negative values given the right response from stretching. The latter would constitute a rarely found property. This has (only?) been reported indirectly for bulk graphite by Deng et al. [13] where the friction kept increasing during the unloading phase. Check for other cases and what I can really say here.

To the best of our knowledge, kirigami has not yet been implemented to alter the frictional properties of a nanoscale system. However, in a recent paper by Liefferink et al. [14](2021) it is reported that macroscale kirigami can be used to dynamically control the macroscale roughness of a surface through stretching which was used to change the frictional coefficient by more than one order of magnitude. This supports the idea that kirigami designs can be used to alter friction, but we believe that taking this concept to the nanoscale regime would involve a different set of underlying mechanisms and thus contribute to new insight in this field.

## 1.2 Goals

In this thesis we investigate the possibility to alter and control the frictional properties of a graphene sheet through application of kirigami inspired cuts and stretching of the sheet. With the use of MD simulations we evaluate the friction properties under different physical conditions in order to get insight into the prospects of this field. By evaluating variations of two kirigami inspired patterns and a series of random walk generated patterns we create a dataset containing information of the frictional properties associated with each design under different load and stretch conditions. We apply ML to the dataset and use an accelerated search approach to

optimize for different properties of interest. The subtask of the thesis are presented more comprehensively in the following.

1. Define a sheet indexing that allows for an unqiue mapping of patterns between a hexagonal graphene lattice representation to a matrix representation suited for numerical analysis.
2. Design a MD simulation procedure to evaluate the frictional properties of a given graphene sheet under specified physical conditions such as load, stretch, temperature etc.
3. Find and implement suitable kirigami patterns which exhibit out-of-plane buckling under tensile load. This includes the creation of a framework for creating variations within each pattern class. Additionally create a procedure for generating different styles of random walk patterns.
4. Perform a pilot study of a representative subset of patterns in order to determine appropriate simulation parameters to use for the further study along with an analysis of the frictional properties shown in the subset.
5. Create a dataset consisting of the chosen kirigami variations and random walk patterns and analyse data trends.
6. Train a neural network to map from the design space to physical properties such as mean friction, maximum friction, contact area etc. and evaluate the performance.
7. Perform an accelerated search optimizing for interesting frictional properties using the ML model. This should be done both through the pattern generation procedures and by following a genetic algorithm approach.
8. Use the most promising candidtes from the accelerated search to investigate the prospects of creating a nanomachine setup which exhibits a negative friction coefficient.
9. Study certain designs of interest with the scope of revealing underling mechanism. This includes simple correlation analysis but also a visualization of feature and gradient maps of the ML network.

Is the list of subtask to specific? Some of the details here might be better suited for the thesis structure section.

## 1.3 Contributions

What did I actually achieve

## 1.4 Thesis structure

How is the thesis structured.

# Part I

# Background Theory

# Chapter 2

# Machine Learning

In this thesis machine learning will serve as a numerical tool for evaluating and exploring the frictional behavior of various Kirigami designs. We will generate data using MD simulations which serve as a ground truth for the training of a machine learning model. If successful, we can utilize such a model to predict the frictional behavior of unseen configurations. The machine learning predictions will be a lot faster than carrying out a complete MD simulation and thus this can be used to accelerate the search through a new set of configurations. It is not obvious that the machine learning model can readily capture the physical mechanisms in our system. Hence, the attempt to model the system with machine learning also has value in terms of revealing the usefulness of such methods to this problem. We aim to implement a rather traditional machine-learning approach. In this chapter we introduce the key concept behind machine learning and some of the relevant concepts and techniques relevant to our implementation.

## 2.1 Neural network

The neural network, or more precisely the *feed forward dense neural network*, is one of the original concepts in machine learning arising from the attempt of mimicking the way neurons work in the brain [15, 16]. The neural network can be considered as three major parts: The input layer, the so-called *hidden layers* and finally the output layer as shown in Fig. 2.1. The input is described as a vector $\mathbf{x} = x_0, x_1, \ldots, x_{n_x}$ where each input $x_i$ is usually denoted as a *feature*. For our task we will consider the Kirigami configuration, load and stretch of the system as input features on which we want the model to base its prediction. The input features are densely connected to each of the *nodes* in the first hidden layers as indicated by straight lines in Fig. 2.1. Each line represents a weighted connection that can be adjusted to configure the importance of that feature. Similar dense connections run through all the hidden layers to the final output layer. For a given note $a_j^{[l]}$ in layer $l$ will process the input from layer $l-1$ as

$$a_j^{[l]} = f\left(\sum_i w_{ij}^{[l]} a_i^{[l-1]} + b_j^{[l]}\right),$$

where $w_{ij}^{[l]}$ is the weight connection node $a_i^{[l-1]}$ of the previous layer to the node $a_j^{[l]}$ in the current layer. Note that the choice of denoting this weight to belong to layer $l$ as opposed $l-1$ is simply a notation choice. $b_j^{[l]}$ denotes a bias and $f(\cdot)$ the *activation function*. The activation function is often chosen to give a non-linear mapping of the input to each node. Without this, the network will only be capable of approximate linear functions [15]. Two common activation functions are the *sigmoid*, mapping the input to the range $(0, 1)$, and the ReLU which cuts off negative values and maps positive linearly

$$\text{Sigmoid:} \quad f(z) = \frac{1}{1e^{-z}}, \qquad \text{ReLU:} \quad f(z) = \begin{cases} z \text{ for } z > 0 \\ 0 \text{ for } z \leq 0. \end{cases}$$

Often the same activation function is used throughout the network, except for the output layer where the activation function is usually omitted or the sigmoid is used for classification tasks. The whole process of sending

data through the model is called *forward propagation* and constitutes the mechanism for mapping an input $\mathbf{x}$ to the model output *vêcy*. In order to get useful predictions we must *train* the model which involves tuning the model parameters, the weight and biasses.

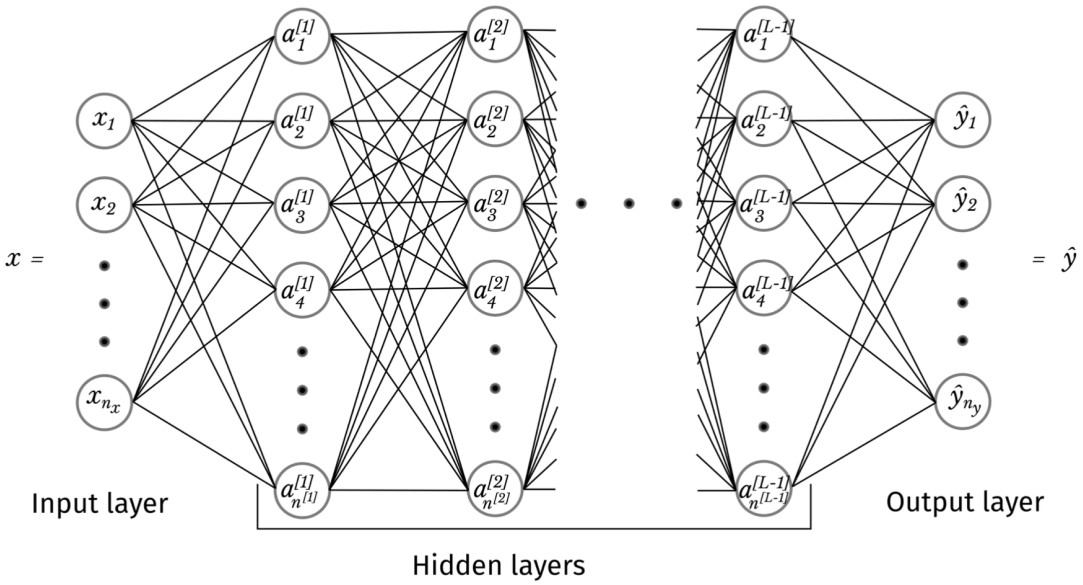


**Figure 2.1:** From overleaf IN400

The model training relies on two core concepts: *backpropagation* and *gradient descent* optimization. We define the error associated with a model prediction, otherwise known as the *loss*, through the *loss function* $L$ that evaluates the model output $\hat{\mathbf{y}}$ against the true value $\mathbf{y}$. For a continuous scalar output, we might simply use the mean squared error (MSE)

$$L_{\text{MSE}} = \frac{1}{N_y}\sum_{i=1}^{N}(y_i - \hat{y}_i)^2.$$

For a binary classification problem, meaning that the true output is True or False (1 or 0), a common choice is binary cross entropy (BSE)

$$L_{\text{BSE}} = -\sum_{i=1}^{n}\Big[y_i \log(\hat{y}_i) + (1-y_i)\log(1-\hat{y}_i)\Big] = \sum_{i=1}^{n}\begin{cases} -\log(\hat{y}_i), & y_i = 1 \\ -\log(1-\hat{y}_i), & y_i = 0. \end{cases}$$

The cross-entropy loss can be derived from a maximum likelihood estimation SOURCE. Without going into details with the derivation we can convince ourselves that the error is minimized for the correct prediction and maximized for the worst prediction. When $y_i = 1$ we get the negative term $-\log(\hat{y}_i)$ where a correct prediction $\hat{y}_i \to 1$ yields a loss contribution $L_i \to 0$. For a wrong prediction $\hat{y}_i \to 0$ the loss contribution will diverge $L_i \to \infty$. Similar applies to the case of $y_i = 0$ with opposite directions.

Given a loss function, we can calculate the loss gradient $\nabla_\theta L$ with respect to each of the weights and biases in the model. This gradient expresses how each parameter is connected to the loss. The overall idea is then to "nudge" each parameter in the right direction. We generally denote a full cycle of forward and backpropagation and an update to the parameters as an epoch. We calculate the updated parameter $\theta_t$ for epoch $t$ using gradient descent

$$\theta_t = \theta_{t-1} - \eta\nabla_\theta L(\theta_t).$$

Gradient descent is analog to taking a step in parameter space in the direction that yields the biggest decrease in the loss. If we imagine a simplified analog with only two parameters $\theta_1$ and $\theta_2$ we can think of this as the act

of stepping perpendicular to the contour lines shaped by the loss function as shown in Fig. 2.2a. Notice however that models in general contain on the order of $10^6 - -10^9$ parameters FACT CHECK, but this might get a bit harder to visualize. The length of each step is proportional to the gradient magnitude and the learning rate $\eta$. There are three main flavors to the gradient descent: Batch, stochastic and mini-batch gradient descent. In batch gradient descent we simply calculate the gradient based on the whole dataset by averaging the contribution from each data point before updating the parameters. This gives the most robust estimate of the gradient and thus the most direct path through parameter space in terms of minimizing the loss function as indicated in Fig. 2.2a. However, for big datasets, this calculation can be computationally heavy as it must carry the entire dataset in memory at once. A solution to this issue is provided by stochastic gradient descent (SGD) which considers only one data point at a time. Each data point is chosen randomly and the parameters are updated based on the corresponding gradient. This leads to more frequent updates of the parameters which will results in a more "noisy" path through parameter space with respect to minimizing the loss as shown in Fig. 2.2b. In some situations, this might compromise the precision but the noisiness makes it more likely to escape local minima in the loss space. The mini-batch gradient descent serves as a middle ground between the above methods by dividing the full dataset into a subset of mini-batches. Each parameter update is then based on the gradient within a mini-batch. By choosing a suitable batch size we get the robustness of the (full) batch gradient descent and the computational efficiency and resistance to local minima of the SGD method.

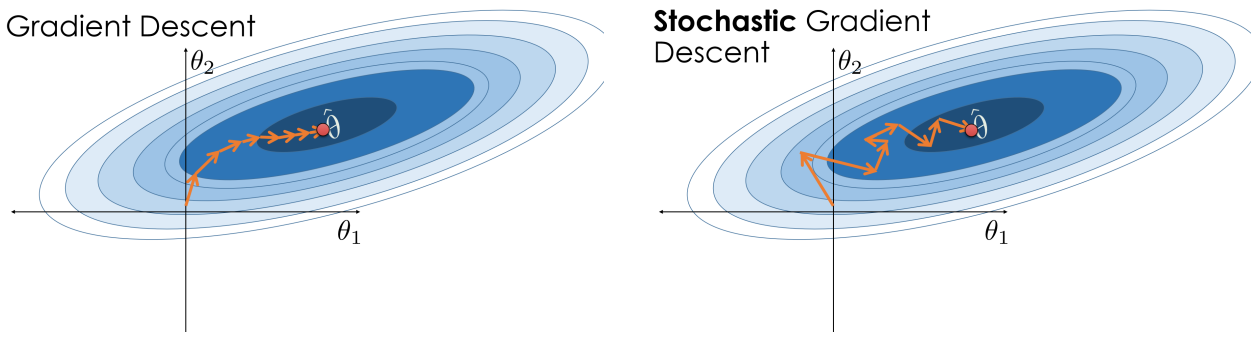


(a) (b)

**Figure 2.2:** TMP

## 2.2 Optimizers

The name *optimizers* covers a variety of gradient descent methods. In our study, we will use the ADAM (adaptive moment estimation). ADAM combines several "tricks in the book" which we will introduce in the following.

One considerable extension of the gradient descent scheme is by the introduction of a momentum term $m_t$ such that we get

$$\theta_t = \theta_{t-1} - m_t, \qquad m_t = \alpha m_{t-1} + \eta \nabla_\theta L(\theta_t) \tag{2.1}$$

with $m_0 = 0$. If we introduce the shorthand $g_t = \nabla_\theta L(\theta_t)$ we find

$$\begin{aligned} m_1 &= \alpha m_0 + \eta g_1 = \eta g_1 \\ m_2 &= \alpha m_1 + \eta g_2 = \alpha^1 \eta g_1 + \eta g_2 \\ m_3 &= \alpha m_2 + \eta g_3 = \alpha^2 \eta g_1 + \alpha \eta g_2 + \eta g_3 \\ &\vdots \\ m_t &= \eta \left( \sum_{k=1}^{t} \alpha^{t-k} g_k \right). \end{aligned} \tag{2.2}$$

Hence $m_t$ is a weighted average of the gradients with an exponentially decreasing weight. This act as a memory of the previous gradients and aid to pass local minima and to some degree plateaus in the loss space. A variation

of momentum can be achieved with the introduction of the exponential moving average (EMA) which builds on the recursion

$$\begin{aligned}
\mathrm{EMA}(g_1) &= \alpha \overbrace{\mathrm{EMA}(g_0)}^{\equiv 0} + (1-\alpha) g_1 \\
\mathrm{EMA}(g_2) &= \alpha \mathrm{EMA}(g_1) + (1-\alpha) g_2 \\
&\vdots \\
\mathrm{EMA}(g_t) &= \alpha \mathrm{EMA}(g_{t-1}) + (1-\alpha) g_t = \sum_{k=0}^{t} \alpha^{t-k} (1-\alpha) g_t,
\end{aligned}$$

which is similar to that of momentum Eq. (2.2), but with the explicit weighting by $(1-\alpha)$.

The second moment of the exponential moving average is utilized in the root mean square propagation (RMSProp) method which is motivated by the issue of passing long plateaus in the loss space. Since the size of the updates are proportional to the norm of the gradient

$$\theta_{t+1} = \theta_t - \eta g_t \implies ||\theta_{t+1} - \theta_t|| = \eta ||g_t||,$$

we might get the idea of normalizing the gradient step by dividing with the norm $|||g_t|$. However, this does not immediately solve the problem of long plateaus as we need to consider multiple past gradients which is then accommodated by the use of the EMA. When reentering a steep region again we need to "quickly" downscale the gradient steps again which can be achieved by using the squared norm $||g_t||^2$ for the EMA which makes it more sensitive to outliers. The RMSProp update scheme then becomes

$$\theta_t = \theta_{t-1} - \eta \frac{g_t}{\sqrt{\mathrm{EMA}(||g_t||^2)} + \epsilon}, \tag{2.3}$$

where $\epsilon$ is simply a small number to avoid division by zero issues.

ADAM merges the idea of first order EMA for the momentum $m_t$, and the second order EMA $v_t$, as used in the root mean square propagation technique in Eq. (2.3)

$$\begin{aligned}
m_t &= \beta_1 m_{t-1} + (1-\beta_1) g_t, \\
v_t &= \beta_2 v_{t-1} + (1-\beta_2) g_t^2.
\end{aligned}$$

Since these are initially set to zero we can correct a bias towards zero by a scaling term $(1-\beta_1^t)$ and $(1-\beta_2^t)$ respectively such that the ADAM scheme becomes

$$\theta_{t+1} = \theta_t - \eta \frac{\hat{m}_t}{\sqrt{\hat{v}_t} + \epsilon}, \qquad \hat{m}_t = \frac{m_t}{1-\beta_1^t}, \qquad \hat{v}_t = \frac{v_t}{1-\beta_2^t}. \tag{2.4}$$

### 2.2.1 Weight decay

By adding a so-called *regularization* to the loss function we penalize high magnitudes of the model parameters. This is motivated by the idea of preventing overfitting in the modeling. The most common way to do this is by L2 regularization, adding the squared $l^2$ norm $||\theta||_2^2$, where $||\theta||_2 = \sqrt{\theta_1^2 + \theta_2^2 + \ldots}$, to the model. The new loss and gradient then become

$$\begin{aligned}
L_{l^2}(\theta) &= L(\theta) + \frac{1}{2}\lambda ||\theta||_2^2 \\
\nabla_\theta L_{l2}(\theta) &= \nabla_\theta L(\theta) + \lambda \theta,
\end{aligned} \tag{2.5}$$

where $\lambda$ is the weight decay parameter $\in [0, 1]$. The name *weight decay* relates to the fact that some practitioners only apply this penalty to the weights in the model, but we will include the biases as well (standard in PyTorch). From the gradient in Eq. (2.5) we find that the original gradient descent scheme becomes

$$\begin{aligned}
\theta_{t+1} &= \theta_t - \eta g_t - \eta \lambda \theta_t \\
&= \theta_t \underbrace{(1 - \eta\lambda)}_{\text{Weight decay}} - \eta g_t.
\end{aligned}$$

Thus we can see that choosing a high weight decay (towards 1) will downscale the model parameters.

### 2.2.2 Parameter distributions

In order to get good training conditions it has been found that the initial distribution of weights and biases matters. First of all we want to initilize a random set of weights since the weights would otherwise undergo the same tuning during gradient descent. Further, we want to avoid the extreme cases of vanishing or exploding gradients. We want to have a zero mean of the gradients for a given layer and a gradient variance across a layer similar for all layers. This is accommodated by scaling the initial weights to meet the same requirements. This depends on the number of input nodes to a given layer and the activation functions used. For instance, when using the RELU activation function it was found that the single standard deviation will go as $\sim \sqrt{\text{input nodes}}/\sqrt{2}$ and thus we scale each layer by this value. This is part of the Kaiming initialization scheme which is standard in Pytorch.

Batch normalization is a technique to speed up and make the training more stable. Weights and biases are modified throughout training meaning that the input to a given node in some layer within the model will also most likely get a changing range of values. By scaling the input for a given layer, for each batch, we can mitigate this problem and make for a standardized value range. The model can then "focus" on the distribution of the input without dealing with an overall shift in values. For layer $l$ we calculate the mean $\mu^{[l]}$ and variance $(\sigma^{[l]})^2$ across the layer with nodes $x_1^{[l]}, x_2^{[l]}, \ldots, x_d^{[l]}$ for each mini-batch of size $m$ as

$$\mu^{[l]} = \frac{1}{m}\sum_i z^i, \qquad (\sigma^{[l]})^2 = \frac{1}{m}\sum_i^d (x^i - \mu)^2.$$

We then perform normal scaling of the inputs within the batch

$$\hat{x}_i^{[l]} = \frac{x_i^{[l]} - \mu^{[l]}}{\sqrt{(\sigma^{[l]})^2 + \epsilon}},$$

where $\epsilon$ is a small number to ensure numerical stability (similar to RMSProp). In the final step the input values are rescaled as

$$? = \gamma^{[l]}\hat{x}_i^{[l]} + \beta^{[l]}$$

with trainable parameters $\gamma$ and $\beta$.

### 2.2.3 Learning rate decay strategies

## 2.3 Convolutional Neural Network

Convolutional Neural Network (CNN) builds on feed forward neural network, but is specialized for spatial inputs such as images. The neural network applies a so-called *kernel* which is a filter sliding over the image. for a multi-channel image, such as the standard RGB containing a channel for red, green and blue colors, the kernel must have a depth that matches this. The input is processed as a dot product between similar channels in the input and the kernel for which the resulting values are summed and added with a single bias set for the whole kernel as illustrated in Fig. 2.4. Each kernel represents as a set of trainable weights and a bias. Often multiple kernels is applied to the input which results in an increasing number of channels throughout the model. On the otherside the spatial input is down-scaled. By controlling the *stride*, the translation of the filter between each convolution, we can alter the amount of down-scaling. If we keep the stride and apply a paddin around the input, using zeroes or extending the edge for instance, we can also choose to preserve the spatial size in the convolution. The spatial size is given by the formula

$$N_{i+1} = \left\lfloor \frac{N_i - F + 2P}{S} + 1 \right\rfloor, \tag{2.6}$$

for padding $P$, stride $S$, spatial size of the kernel filter $F$, spatial size of input $N_i$ and spatial size of output $N_{i+1}$. The down-samling feature is often ... through a pooling layer. A pooling layer process the input by taking the mean (mean pooling) or the max value (max pooling) in the filter as it slides over the input. This is often used after a convolution meaning that the input is given as the resulting feature map. For instance, by making a max pooling of size $2 \times 2$ by stride two we essentially half the dimensions of the image, but this follows Eq. (2.6).

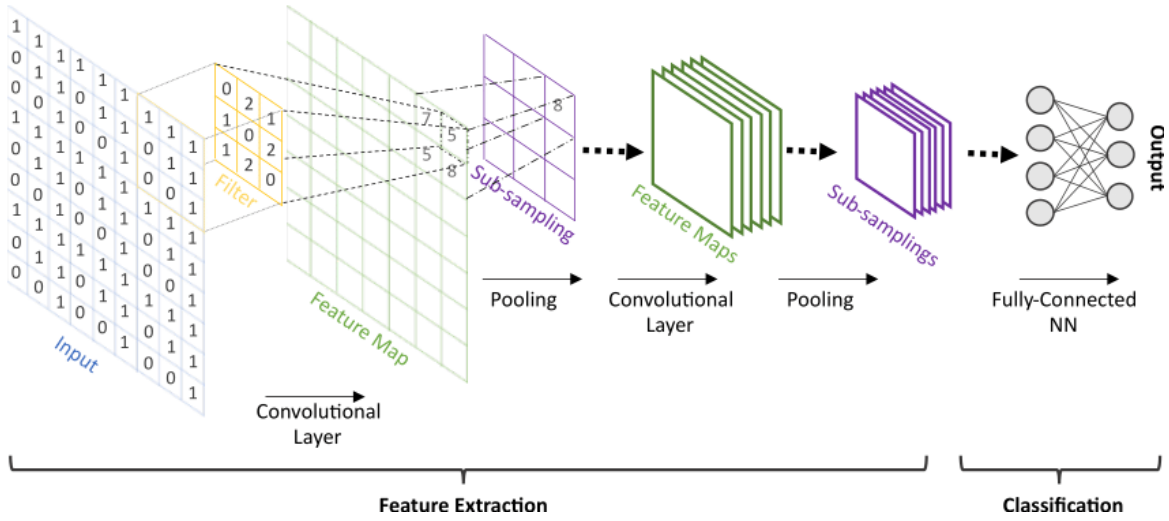


**Figure 2.3:** TMP

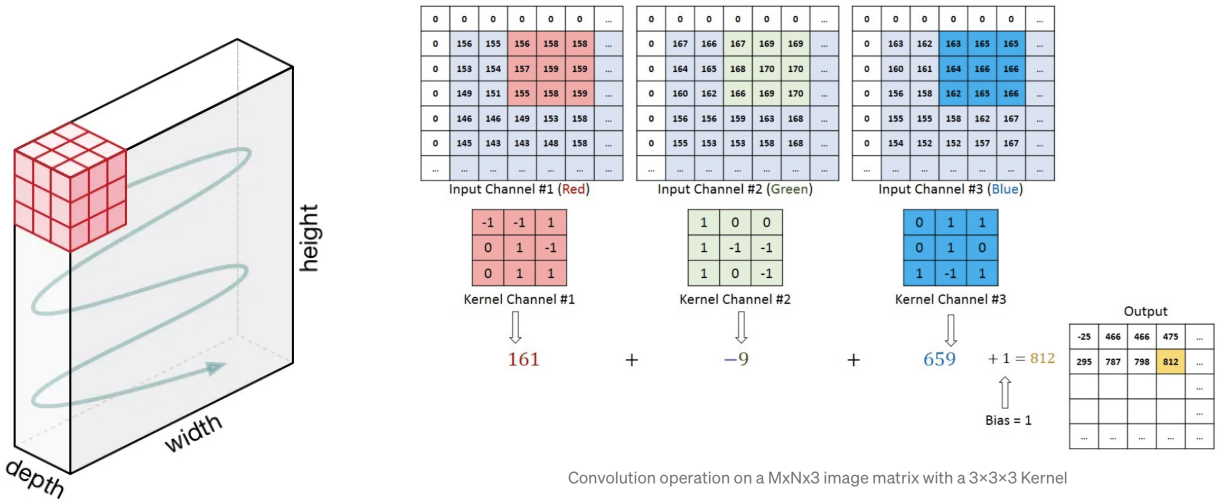


**(a)** **(b)**

**Figure 2.4:** TMP

For a convolution process, we often consider the *receptive field*. The receptive field relates to the spatial size of the input that affects a given node in the feature map at a given layer of the model. In Fig. 2.5 the receptive field is illustrated of a 1D representation of convolutional with a filter of stride 1 and filter width 2. Going from the output and backwards, we see that the output relates to two nodes in the previous last hidden layer. Each of these nodes is connected to two nodes in the layer before that, however with on of them being the same due to the stride of 1. By back tracking all the way to the input we see that this corresponds to a receptive field of $D = 5$. By increasing the filter size and the stride the 2D receptive field will grow a lot faster than shown in this simple 1D example. For a receptive field $D$, in a given spatial dimension, a spatial size of the filter $F$, stride $S_i$ (from layer $i$ to $i-1$), layer index: $l = \{1, 2, 3, \cdots, n\}$, we have

$$D_l = D_{l-1} + \left[ (F_l - 1) \cdot \prod_{i=1}^{l-1} S_i \right],$$

with $D_0 = 1$ and $l = 0$ as the input layer. Note that by convention, the product of 0 is 1, so for the first layer, the sum over $S$ is 1. The receptive field is important in understanding the connectivity in the model. The model

output will be completely independent of the inputs and feature maps outside the receptive field. Furthermore, since nodes in the center of the receptive field cones often have multiple connective paths leading to the output, as seen in Fig. 2.5 as well, we differentiate between the theoretical receptive field and the effective receptive field. The effective receptive field will have a Gaussian distribution within the theoretical receptive field due to the fact that the nodes in the center will be more represented as multiple paths connect to the output. Thus we in practice consider the effective receptive field to be smaller than the theoretical. Implementations like dilated convolutions, which make the filter expand in circumference and skipping skipping positions within the filter, can be used to further increase the effective field.

The power of the CNN lies mainly in the ability to carry translational invariance as opposed to a dense neural network. If practice, if you train a dense network to classify cat images and only show images with cats on the left side it will fail horribly when predicting on similar imiages with cats on the right side of the image. The CNN is less proven to such issues as each kernel translates the whole image using the same weights. This is also the reason that the CNN architecture is more parameter efficient. For a dense network it would essentially need to have "cat-detecting" weights and bias configurations for all parts of the input. This forces a dense network to learn similar trends for multiple part of the network in contrast to the CNN.

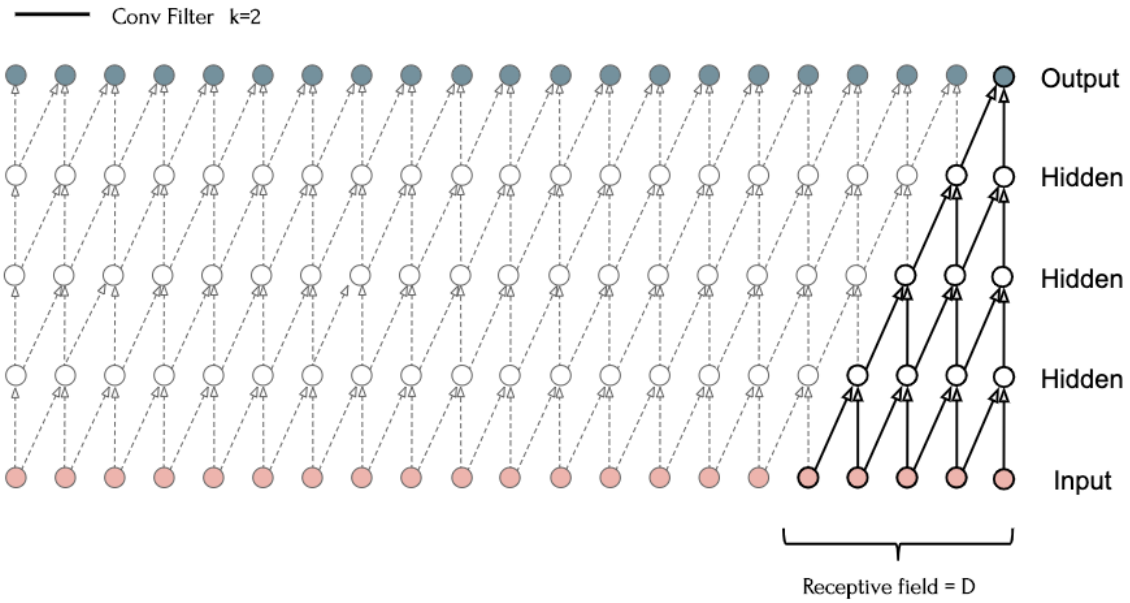


**Figure 2.5:** TMP

## 2.4 Overfitting and underfitting

Underfitting is recognized as a loss curve that continues to decrease slowly. This is highly dependent on the complexity of the model and the learning rate. A to small learning rate will induce underfitting

Overfitting a more complicated to diagnostic. The Dynamics is not as simple as sketched in Fig. 2.6.

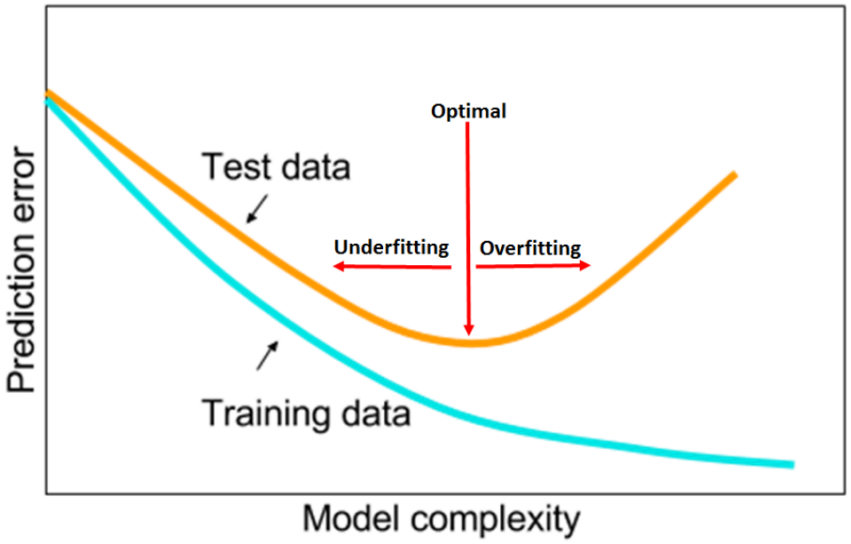


Figure 2: Pictorial explanation of the tradeoff between underfitting and overfitting. Model complexity (the x axis) refers to the capacity or powerfulness of the machine learning model. The figure shows the optimal capacity that falls between underfitting and overfitting.

**Figure 2.6:** TMP [17]

## 2.5 MOre stuff

1. Talk about training, validation and test split
2. What about performance measuring?

## 2.6 Hypertuning

Training a machine learning model revolves around tuning the model parameters consisting of mainly weights and biases. By following the general idea by the gradient descent approach we can get complex models able to give complex predictions. However, a handful of so-called *hyper-parameters* remain for us to decide. First of all we must decide on an architecture for the model. This includes high level considerations as for instance to use neural network or a convolutional network, but also lower level considerations like the depth of the model and number of nodes/channels per layer. The choice of loss function and optimizers come with hyperparameters like learning rate, momentum and weight decay. As N. Smith [17] puts it: "Setting the hyper-parameters remains a black art that requires years of experience to acquire". In the following, we will review some general approaches to the hypertuning presented in [17]. The traditional way is to perform a grid-search of multiple training sessions with different combinations of hyper-parameters. This can be computationally expensive. In addition, hyper-parameters will depend on each other, the data and the architecture which can realistically be searched at the same time.

N. Smith points to the fact that validation loss can by examined early on for clues of either underfitting or overfitting. For the learning rates one can use an increasing learning rate scheme for the so-called *learning rate range test* (LR range test). One specifies a minimum and a maximum learning rate boundaries and a learning rate step size. This can be done both for linear increasing or decreasing learning rate, which proved to give similar results [17] Jastrzebski et al. (2017b). We choose the linear increasing version for simplicity. In the LR range test training then starts form the lowest learning rate which is increased in small steps during a pre-training. The stepsize can be number of mini-batch iterations, and does not have to stick to epochs. For small learning rates the network will converge slowly. As the learning rate apporahces an appropriate size the

convergence more strongly. Eventually the convergence will stop and the loss will increase again as the learning rates becomes to high (show harmonic potential big learning rate example somewhere?). The learing rates at the point of divergence indicate an upper bound the learning rate that can be used with a cyclic learing rate scheme. One have to set the upper bound a bit lower than this to avoid divergence in practice. The steepest decline of the validation curve can be used as an estimate for the best constant learning rate choice.

Next up, is momentum. Momentum and learning rates effect each other and since the learning rate is regarded as one of the most important hyper-parameters to tune SOURCE momentum is also important. We want to set both learning rate and momentum as large as possible without causing instabilities to the training. Momentum is designed to accelerate the training process but the effect on updating the weights is of the same magnitude as learning rate as present from Eq. (2.1). Experiments show that finding a the right momentum from momentum range test is not useful. Thus, short runs with different values of momentum, on the range 0.9–0.99, can be done to find the best choice of momentum. The learning rate and momenmtum will however often be inversely dependent. Choosing a high learning rate will result in a slightly lower momentum being appropriate and vice versa. Thus, when using a cycling learning rate scheme one should adopt a cyclic momentum scheme as well with decreasing momentum for increasing learning rate. Choosing a lower momentum of 0.80–0.85 often gives similar stabile results.

Finally we address the weight decay. N. Smith reports that weight decay is not similar to learning rate and momentum as it is better to choose a constant weight decay through the training. This will be dependent on the model complexity and he suggest doing a grid-search for values such as 0, $10^{-6}$, $10^{-5}$ and $10^{-4}$ for complex architecture and $10^{-4}$, $10^{-3}$ and $10^{-2}$ for more shallow architectures. Choosing the weight decay on the scale of exponential exponents is often good enough as the sensitivity to precise factors is not found to be highly important. The optimal weight decay will depend on your learning rate and momentum scheme.

## 2.7 Prediction explanation

Looking at feature maps and gradient maps.

## 2.8 Accelerated search using genetic algorithm

### 2.8.1 Markov-Chain Accelerated Genetic Algorithms

#### 2.8.1.1 Talk about traditional method also?

#### 2.8.1.2 Implementing for 1D chromosone (following article closely)

We have the binary population matrix $A(t)$ at time (generation) $t$ consisting of $N$ rows denoting chromosones and with $L$ columns denoting the so-called locus (fixed position on a chromosome where a particular gene or genetic marker is located, wiki). We sort the matrix rowwise by the fitness of each chromosono evaluated by a fitness function $f$ such that $f_i(t) \leq f_k(t)$ for $i \geq k$. We assume that there are a transistion probability between the current state $A(t)$ and the next state $A(t+1)$. We consider this transistion probability only to take into account mutation process (mutation only updating scheme). During each generation chromosones are sorted from most to least fitted. The chromosone at the $i$-th fitted place is assigned a row mutation probability $a_i(t)$ by some monotonic increasing function. This is taken to be

$$a_i(t) = \begin{cases} (i-1)/N', & i-1 < N' \\ 1, & \text{else} \end{cases}$$

for some limit $N'$ (refer to first part of article talking about this). We use $N' = N/2$. We also defines the survival probability $s_i = 1 - a_i$. In thus wau $a_i$ and $s_i$ decide together whether to mutate to the other state (flip binary) or to remain in the current state. We use $s_i$ as the statistical weight for the $i$-th chromosone given it a weight $w_i = s_i$.
Now the column mutation. For each locus $j$ we define the count of 0's and 1's as $C_0(j)$ and $C_1(j)$ resepctively. These are normalized as

$$n_0(j,t) = \frac{C_0(j)}{C_0(j) + C_1(j)}, \quad n_1(j,t) = \frac{C_1(j)}{C_0(j) + C_1(j)}.$$

These are gathered into the vector $\mathbf{n}(j,t) = (n_0(j,t), n_1(j,t))$ which characterizes the state distribution of $j$-th locus. In order to direct the current population to a preferred state for locus $j$ we look at the highest weight of row $i$ for locus $j$ taking the value 0 and 1 respectively.

$$C_0'(j) = \max\{W_i | A_{ij} = 0;\ i = 1, \cdots, N\}$$
$$C_1'(j) = \max\{W_i | A_{ij} = 1;\ i = 1, \cdots, N\}$$

which is normalized again

$$n_0(j,t+1) = \frac{C_0'(j)}{C_0'(j) + C_1'(j)}, \quad n_1(j,t+1) = \frac{C_1'(j)}{C_0'(j) + C_1'(j)}.$$

The vector $\mathbf{n}(j,t+1) = (n_0(j,t+1), n_1(j,t+1))$ then provides a direction for the population to evolve against. This characterizes the target state distribution of the locus $j$ among all the chromosones in the next generation. We have

$$\begin{bmatrix} n_0(j,t+1) \\ n_1(j,t+1) \end{bmatrix} = \begin{bmatrix} P_{00}(j,t)\ P_{10}(j,t) \\ P_{01}(j,t)\ P_{11}(j,t) \end{bmatrix} \begin{bmatrix} n_0(j,t) \\ n_1(j,t) \end{bmatrix}$$

Since the probability must sum to one for the rows in the P-matrix we have

$$P_{00}(j,t) = 1 - P_{01}(j,t), \quad P_{11}(j,t) = 1 - P_{10}(j,t)$$

These conditions allow us to solve for the transition probability $P_{10}(j,t)$ in terms of the single variable $P_{00}j,t$.

$$P_{10}(j,t) = \frac{n_0(j,t+1) - P_{00}(j,t) n_0(j,t)}{n_1(j,t)}$$
$$P_{01}(j,t) = 1 - P_{00}(j,t)$$
$$P_{11}(j,t) = 1 - P_{10}(j,t)$$

We just need to know $P_{00}(j,t)$. We start from $P_{00}(j,t=0) = 0.5$ and then choose $P_{00}(j,t) = n_0(j,t)$

#### 2.8.1.3 Repair function

Talk about it here or in random walk section?

# Part II

# Simulations

# Appendices

# Appendix A

# Appendix B

# Appendix C

# Bibliography


[1]E. Gnecco and E. Meyer, *Elements of friction theory and nanotribology* (Cambridge University Press, 2015).

[2]Bhusnan, "Introduction", in *Introduction to tribology* (John Wiley & Sons, Ltd, 2013) Chap. 1, 1–?

[3]H.-J. Kim and D.-E. Kim, "Nano-scale friction: a review", International Journal of Precision Engineering and Manufacturing **10**, 141–151 (2009).

[4]K. Holmberg and A. Erdemir, "Influence of tribology on global energy consumption, costs and emissions", Friction **5**, 263–284 (2017).

[5]B. Bhushan, "Gecko feet: natural hairy attachment systems for smart adhesion – mechanism, modeling and development of bio-inspired materials", in *Nanotribology and nanomechanics: an introduction* (Springer Berlin Heidelberg, Berlin, Heidelberg, 2008), pp. 1073–1134.

[6]P. Z. Hanakata, E. D. Cubuk, D. K. Campbell, and H. S. Park, "Accelerated search and design of stretchable graphene kirigami using machine learning", Phys. Rev. Lett. **121**, 255304 (2018).

[7]P. Z. Hanakata, E. D. Cubuk, D. K. Campbell, and H. S. Park, "Forward and inverse design of kirigami via supervised autoencoder", Phys. Rev. Res. **2**, 042006 (2020).

[8]L.-K. Wan, Y.-X. Xue, J.-W. Jiang, and H. S. Park, "Machine learning accelerated search of the strongest graphene/h-bn interface with designed fracture properties", Journal of Applied Physics **133**, 024302 (2023).

[9]Y. Mao, Q. He, and X. Zhao, "Designing complex architectured materials with generative adversarial networks", Science Advances **6**, eaaz4169 (2020).

[10]Z. Yang, C.-H. Yu, and M. J. Buehler, "Deep learning model to predict complex stress and strain fields in hierarchical composites", Science Advances **7**, eabd7416 (2021).

[11]A. E. Forte, P. Z. Hanakata, L. Jin, E. Zari, A. Zareei, M. C. Fernandes, L. Sumner, J. Alvarez, and K. Bertoldi, "Inverse design of inflatable soft membranes through machine learning", Advanced Functional Materials **32**, 2111610 (2022).

[12]S. Chen, J. Chen, X. Zhang, Z.-Y. Li, and J. Li, "Kirigami/origami: unfolding the new regime of advanced 3D microfabrication/nanofabrication with "folding"", Light: Science & Applications **9**, 75 (2020).

[13]Z. Deng, A. Smolyanitsky, Q. Li, X.-Q. Feng, and R. J. Cannara, "Adhesion-dependent negative friction coefficient on chemically modified graphite at the nanoscale", Nature Materials **11**, 1032–1037 (2012).

[14]R. W. Liefferink, B. Weber, C. Coulais, and D. Bonn, "Geometric control of sliding friction", Extreme Mechanics Letters **49**, 101475 (2021).

[15]J. Lederer, *Activation functions in artificial neural networks: a systematic overview*, 2021.

[16]P. Shankar, "A review on artificial neural networks", **3**, 166–169 (2022).

[17]L. N. Smith, *A disciplined approach to neural network hyper-parameters: part 1 – learning rate, batch size, momentum, and weight decay*, 2018.